NANO LETTERS

LETTER

pubs.acs.org/NanoLett

Thermal transport across Twin Grain Boundaries in Polycrystalline Graphene from Nonequilibrium Molecular Dynamics Simulations

Akbar Bagri,[†] Sang-Pil Kim,[†] Rodney S. Ruoff,[‡] and Vivek B. Shenoy*[,†]

[†]School of Engineering, Brown University, Providence, Rhode Island 02912, United States

[‡]Department of Mechanical Engineering and the Texas Materials Institute, University of Texas, Austin, Texas 78712, United States

ABSTRACT: We have studied the thermal conductance of tilt grain boundaries in graphene using nonequilibrium molecular dynamics simulations. When a constant heat flux is allowed to flow, we observe sharp jumps in temperature at the boundaries, characteristic of interfaces between materials of differing thermal properties. On the basis of the magnitude of these jumps, we have computed the boundary conductance of twin grain boundaries as a function of their misorientation angles. We find the boundary conductance to be in the range 1.5×10^{10} to 4.5×10^{10} W/(m^2 K), which is significantly higher than that of any other thermoelectric interfaces reported in the literature. Using the computed values of boundary conductances, we have identified a critical grain size of 0.1 μm below which the contribution of the tilt boundaries to the conductivity becomes comparable to that of the contribution from the grains themselves. Experiments to test the predictions of our simulations are proposed.

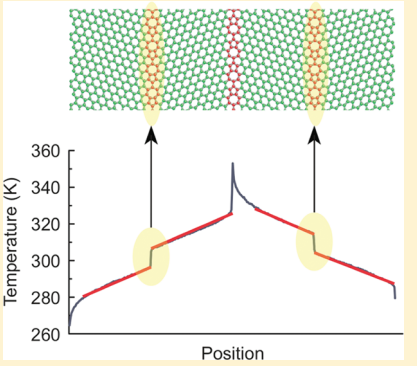

KEYWORDS: Thermal conductivity, polycrystalline graphene, phonon transport, Kapitza conductance

Graphene is a material consisting of a single atomic carbon layer arranged in a two-dimensional (2D) honeycomb lattice, discovered in 1969[1] and studied extensively since then[2] by the surface science community. It has attracted widespread interest for both its novel electronic properties and Dirac band dispersion as well as its broad application potential.[2−9] Due to its high mobility, it also has been proposed to show great promise for high-speed switching in microwave and terahertz devices[10−12] and terahertz plasmon amplification.[13] Graphene exhibits exceptional electronic, thermal, optical, and mechanical properties.[6,14] Growing large-area, single-layer graphene sheets, however, remains a major challenge. Recently, a chemical vapor deposition (CVD) technique has been devised that exploits the low solubility of carbon in metals such as nickel[15,16] and copper[17,18] in order to grow graphene on metal foils. A consequence of this technique is that the large-area graphene sheets typically contain grain boundaries, because each grain in the metallic foil serves as a nucleation site for individual grains of graphene.[17] Thus in applications that employ large area CVD-grown graphene, the effect of grain boundaries on the fundamental physical properties must be understood.

The structures of grain boundaries in graphene have recently been studied both theoretically[19−22] and experimentally.[23,24] The influence of grain boundaries on the electronic[19] and mechanical[22] properties of graphene has also been considered. However, to date, there are no studies that consider the role of grain boundaries on the thermal conductivity of polycrystalline graphene. Here, we study heat transport across tilt grain boundaries in graphene using molecular dynamics simulations. We observe a sharp jump in the temperature across the grain boundary that is typical of an interface between regions with differing thermal properties. By relating the jump in temperature to the heat flux, we are able to extract the thermal boundary resistance (also called Kapitza resistance[25,26]) of the grain boundaries.

In this work, we compute the thermal conductivity using the reverse nonequilibrium molecular dynamics (RNEMD) simulations.[27,28] The idea of the method is to impose a heat flux through the structure under study and to determine the temperature gradient that develops as a consequence of the imposed flux. The heat flux is introduced by continuously transferring energy from a "cold" slab, located at the ends of the simulation cell, to the "hot" slab, located at the middle of simulation cell (refer to Figure 1). This is accomplished by exchanging the velocities of the hottest atom in the cold slab with the coldest atom in the hot slab. The heat flux from the cold region to the hot region due to the exchange of the atoms is given by

$$q = \frac{1}{2tA_{yz}} \sum_{\text{transfer}} \frac{m}{2} \left(v_{\text{hot}}^2 - v_{\text{cold}}^2\right) \qquad (1)$$

where q is the heat flux, t is the total time over which the simulations are carried out, A_{yz} is the cross-sectional area perpendicular to the direction of heat flow, m is the mass of the atoms, v_{hot} and v_{cold} are the velocities of the hottest atom of the cold region and the coldest atom of the hot region, respectively. The factor 2 in the denominator arises because of the periodicity of the

Received: June 23, 2011
Revised: August 18, 2011
Published: August 24, 2011

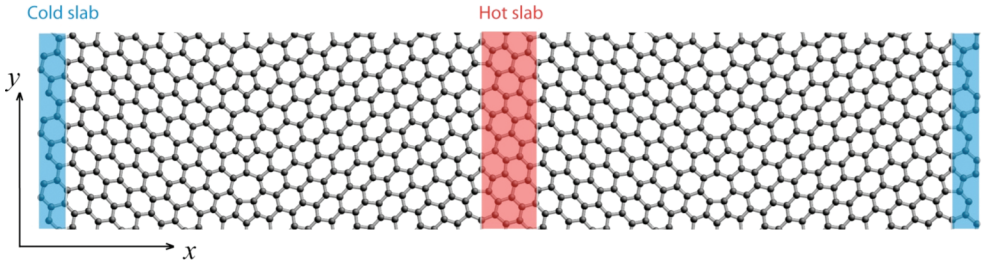

Figure 1. Geometry of the RNEMD simulation box. The cold slabs are placed at the ends of the simulation cell, while the hot slab is located in the middle of the cell.

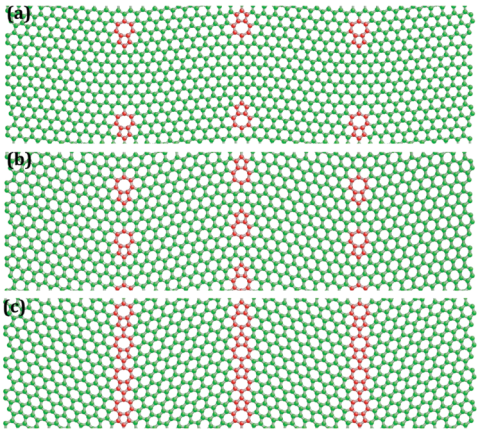

Figure 2. Structure of tilt grain boundaries with misorientation angles of (a) 5.5°, (b) 13.2°, and (c) 21.7°.

system. When the heat flow in the structure reaches the steady state regime, averaging over the heat flux and temperature gradient and using the Fourier's heat conduction equation, the thermal conductivity can be obtained from

$$\langle q \rangle = k\left\langle \frac{dT}{dx} \right\rangle \tag{2}$$

in which k is the thermal conductivity and T is the temperature. The brackets, $\langle\rangle$, indicate the average of the quantities over time as well as over the particles in the simulation cell. The above approach for computing the thermal conductivity of a homogeneous system can also be generalized to the case of a system with defects. In the case of grain boundaries, we consider here imposing a heat flux leads to a "jump" in temperature across the boundary. The jump gives a measure of the boundary conductance (Kapitza conductance) G of the grain boundary through the relation[29]

$$G = \frac{\langle q \rangle}{\Delta T} \tag{3}$$

Furthermore, the temperature profiles that develop across the grains can be analyzed to obtain their thermal conductivity as a function of their orientation.

The structures of tilt grain boundaries in zigzag-oriented graphene are shown in Figure 2 for different grain boundary angles. The grain boundaries consist of repeating five- and seven-membered ring pairs (5-7 pairs) that are separated by several hexagonal rings (hex rings). As the grain boundary angle increases, the number of hex rings separating the 5-7 defects decreases, with the ultimate limit occurring at 21.7° when only a single hex ring separates the periodic 5-7 defects. Therefore, more severe grain boundary angles are composed of higher defect densities. The repeating defect pairs can also be thought of as an array of edge dislocations with horizontal Burgers vectors where the five-membered rings represent the extra plane of atoms. In our simulations, periodic boundary conditions are employed both along the direction of heat flow (x) and perpendicular to the direction of heat flow (y). The atomic interactions are defined by a modified version of the Tersoff potential,[30] which has been recently shown to yield values of the acoustic-phonon velocities that are in excellent agreement with measured data. The potential also provides lattice thermal conductivity values in single-walled carbon nanotubes and graphene that are considerably improved compared to those obtained from the original parameter sets.[31,32]

The atomic coordinates and the overall periodic dimensions of the simulation cell are first optimized using the gradient-based minimization method implemented in the large-scale atomic/molecular massively parallel simulation (LAMMPS) molecular dynamics package[33] in a microcanonical NVE ensemble until the forces on atoms are less than 10^{-8} eV/Å. RNEMD simulations are then carried out on the relaxed structure at room temperature with a time step of 0.5 fs. Before the temperature profiles are computed to infer thermal conductivity, the system is allowed to evolve for 4.4×10^7 MD steps during which the velocities of the atoms in the hot and cold region are exchanged every 100 MD time steps. After the steady state regime is reached, the temperature gradient through the structure is obtained by averaging over 8×10^6 MD steps. The temperature profiles are determined by dividing the structure into slabs that are approximately 10 Å wide.

First, we validate our approach by computing the thermal conductivity of defect-free graphene. The temperature variation obtained in our calculations in this case is shown in Figure 3a. The temperature profile is nonlinear near the hot and cold ends due to finite size effects as noted in previous work[34] and the high thermal conductivity of graphene. Similar temperature profiles have also been noted in carbon nanotubes (CNTs).[35] Care must be taken in the extraction of thermal conductivity from this nonlinear profile, which indicates that thermal transport is not fully diffusive. To obtain the correct diffusive thermal conductivity,[35] we take the temperature gradient of the middle portion between the thermostats to avoid edge effects. Even with this correction, the thermal conductivity inferred from NEMD calculations depends on the size of the system. We find that the conductivity of cells with periodic lengths of 50, 100, and 250 nm, are 532, 898, and 1460 W/(m K), respectively. To calculate the thermal conductivity of 2D graphene sheets, the cross-sectional area is defined as $A_{yz} = wd$, where w is the width of the sheet and d is the thickness (chosen as the interplanar distance in graphite =3.35 Å). The dependence of the thermal conductivity on the length of the

dx.doi.org/10.1021/nl202118d |Nano Lett. 2011, 11, 3917–3921

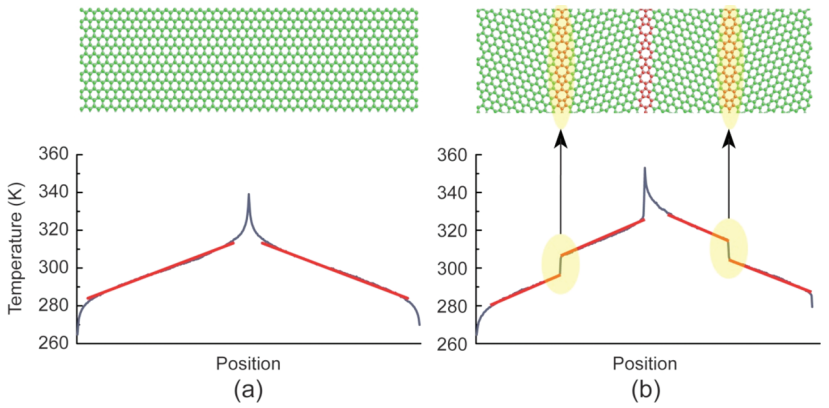

Figure 3. Typical temperature profile through the geometry of (a) graphene and (b) graphene with grain boundaries obtained by using the RNEMD method.

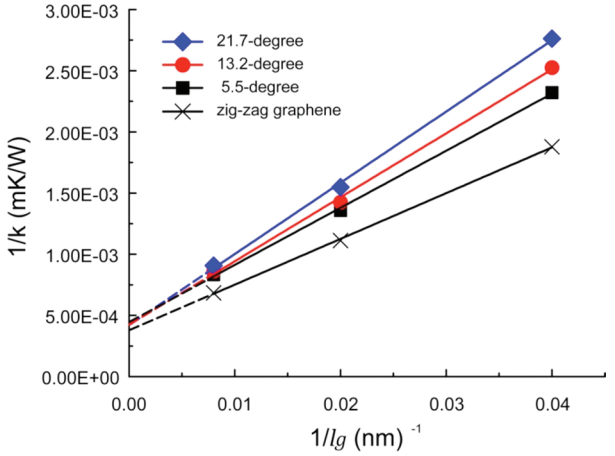

Figure 4. Inverse of thermal conductivity for zigzag-oriented graphene as a function of grain orientation versus the inverse of grain size (l_g). The intercepts for the case of zigzag graphene, 5.5°, 13.2°, and 21.7° oriented grains are 37 × 10^{-5}, 45 × 10^{-5}, 42 × 10^{-5}, and 42 × 10^{-5}, respectively.

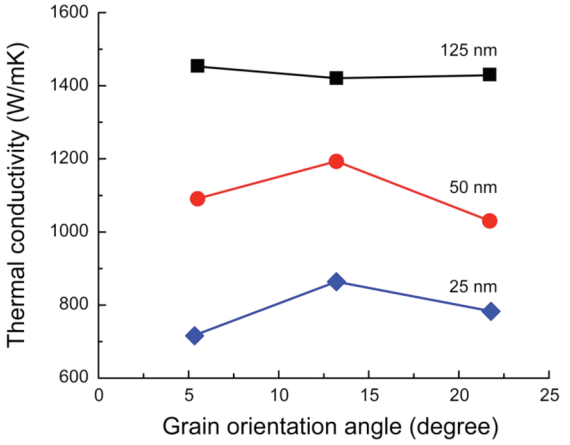

Figure 5. Thermal conductivity of graphene grains of different sizes (25, 50, and 125 nm) versus the orientation of the grain.

simulation cell can be understood by noting that the mean free path of phonons in graphene is of the order of 775 nm,[36] which is bigger than the size of our simulation cells. Therefore, in addition to phonon−phonon scattering, scattering at the heat baths (or boundaries) of the system must be considered. On the basis of the kinetic theory of phonon transport,[37] the thermal conductivity is proportional to the mean free path for phonon scattering. In the case where phonons scatter at the heat reservoir, the effective mean free path is given by

$$\frac{1}{l_{\text{eff}}} = \frac{1}{l_{\text{ph-ph}}} + \frac{1}{l_{\text{g}}} \tag{4}$$

where $l_{\text{ph-ph}}$ denotes phonon−phonon scattering length and l_{g} is scattering length due to the boundaries in a finite system and can be approximated to be the length of the simulation box. On the basis of this relation, the thermal conductivity satisfies the relation

$$\frac{1}{k} \propto \frac{1}{l_{\text{g}}} + \frac{1}{l_{\text{ph-ph}}} \tag{5}$$

which implies that a plot of the inverse of thermal conductivity, k, versus the inverse of the system size, l_{g}, should be a linear curve, the intercept being the thermal conductivity of the infinitely large system. Indeed, the plot of the inverse of the thermal conductivity as a function of the size of the system in Figure 4 confirms this scaling relation. The scaling approach we use here has also been used in earlier work on 3D systems.[34,38] From the intercepts of the plot in Figure 4, we find the thermal conductivity of defect-free graphene along the zigzag direction to be 2650 W/(m K). This result is in excellent agreement with the result (2600 W/(m K)) obtained using the same potential we use here, but a different approach, namely, the nonequilibrium molecular dynamics (NEMD) method.[32] Furthermore, our results agree with the theoretical[39,40] and experimental[41,42] values, which lie in the range 2000−5000 W/(m K). Our results for the thermal conductivity of finite-sized graphene also agree with the results reported in ref 43, where NEMD has been used and the thermal conductivity of graphene of length 29.5 nm was found to be 256 W/(m K).

Next, we consider the temperature profile in the case of graphene with tilt grain boundaries (Figure 3b). We find a nearly linear temperature profile in the grains but observe a jump in the temperature at the grain boundaries. A plot of the thermal conductivity of grains (inferred from the slope of the linear part

dx.doi.org/10.1021/nl202118d |*Nano Lett.* 2011, 11, 3917–3921

Table 1. Temperature Jumps at the Grain Boundaries and Heat Flux (Given in Brackets) for Different Grain Sizes and Angles[a]

grain orientation angle (deg)	25 nm grain size	50 nm grain size	125 nm grain size
5.5	8.13 [1.95 × 10^{11}]	6.18 [1.89 × 10^{11}]	4.40 [1.89 × 10^{11}]
13.2	12.17 [2.15 × 10^{11}]	8.97 [2.13 × 10^{11}]	7.36 [2.19 × 10^{11}]
21.7	12.98 [2.12 × 10^{11}]	10.24 [2.21 × 10^{11}]	7.63 [2.13 × 10^{11}]

[a] Units for the given temperature and heat flux values are kelvin and watt per square meter, respectively.

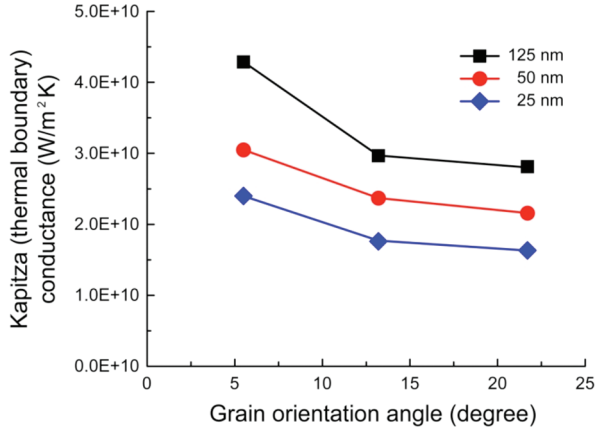

Figure 6. Boundary conductance of grain boundaries as a function of orientation. The curves are labeled by the size of the grains used to compute the boundary conductance.

of the temperature profile) of different orientations as a function of size is plotted in Figure 5. As in the case of zigzag oriented grains, the inverse of the thermal conductivity decreases linearly with the size of the simulation cell. The intercepts of the curves in Figure 4 show that thermal conductivity is anisotropic but only weakly depends on the orientation of the grains (k = 2220, 2380, 2380 W/(m K) for 5.5°, 13.2°, and 21.7° grains, respectively).

The jump in the temperature across the grain boundary can be used in eq 3 to obtain the boundary conductance of the grain boundaries. A summary of these temperature jumps as a function of the grain sizes and angles is given in Table 1. Using the measured jumps, we find that the boundary conductance for the grain boundaries we have considered fall in the range 1.5 × 10^{10} to 4.5 × 10^{10} W/(m^2 K) (refer to Figure 6). These values are 6-to-12, 10-to-50, and 6-to-30 times larger than the boundary conductance's reported for grain boundaries in ultrananocrystalline diamond thin films with grain boundaries on the (001) plane,[44] silicon−silicon (001) Σ29 grain boundaries,[29,45] and the Si−Ge interface with the ⟨100⟩ orientation,[46] respectively. Note that the boundary conductance decreases with increasing misorientation angles of the grain boundaries. This can be qualitatively understood by considering the defect density as a function of grain boundary angle—the higher the misorientation angle, the larger is the density of 5-7 defect pairs per unit length of the boundary, which can lead to an increase in the scattering of phonons and hence a drop in the boundary conductance. We also observe that computed conductance depends slightly on the size of the grains. A similar dependence of the boundary conductance on size has also been reported in refs 29 and 46 for Si−Ge and silicon grain boundaries. This has been attributed to scattering of long wavelength phonons at the heat reservoirs and at the boundaries,[37,47] but a scaling of the conductance with length has not been provided.

Note that when grains are very large in size, the scattering of phonons within the grains will primarily determine the thermal conductivity of the polycrystalline graphene, but with decreasing grain size the contribution to thermal conductivity due to scattering from grain boundaries will become more significant. For the polycrystalline graphene sheet in Figure 2 with grain spacing l_g, the thermal conductivity k_p can be written as

$$k_p^{-1} = k_g^{-1} + (l_g G)^{-1} \quad (6)$$

where k_g is the thermal conductivity of the grain. Using this expression and the computed values of boundary conductance for the tilt boundaries, we can now estimate the critical size of grains below which the contribution from the grain boundaries becomes comparable to the scattering from the grains. This length scale is simply the ratio of the thermal conductivity to the boundary conductance. For the tilt boundaries considered here, this length scale is of the order of 0.1 μm. While a systematic study of the scaling of the thermal conductivity of polycrystalline graphene as a function of grain size has not been reported, the thermal conductivity of exfoliated graphene[48] is generally observed to be higher than the thermal conductivity of CVD graphene.[42] Experiments on graphene with well-controlled grain sizes and orientations can help verify the predictions of this study, namely, the scaling of the boundary conductance (eq 6) and the computed value of boundary conductance as a function of the grain boundary angle. The former can be studied by measuring the overall thermal conductivity of polycrystalline graphene for different grain sizes, while the latter will involve measurement of temperature drop across individual boundaries (once they have been identified using appropriate microscopy techniques).

In summary we have studied thermal transport across tilt grain boundaries in polycrystalline graphene. As in the case of interfaces in the dissimilar materials, we find a jump in temperature at grain boundary when a constant heat flux is applied. We have used this information to extract the boundary conductance, which lies in the range of 1.5 × 10^{10} to 4.5 × 10^{10} W/(m^2 K) in the case of tilt grain boundaries. On the basis of this information, we have identified a critical grain size of about 0.1 μm below which the contribution of tilt boundaries becomes comparable to that of the contribution from the grains themselves. We also note that here we have considered the most common type of tilt boundaries reported in the literature;[19−22] future work on thermal conductance of other types of grain boundaries can shed further light on the thermal transport properties of polycrystalline graphene. Recent experiments have shown that defects such as vacancies and voids tend to segregate at grain boundaries.[23,24] These defects can be expected to further lower the thermal conductance of the boundaries. We hope to consider the effect of these defects in forthcoming publications.

dx.doi.org/10.1021/nl202118d |*Nano Lett.* 2011, 11, 3917–3921

AUTHOR INFORMATION

Corresponding Author
*E-mail: Vivek_Shenoy@brown.edu.

ACKNOWLEDGMENT

The support of the Army Research Office through Contract W911NF-11-1-0171 is gratefully acknowledged.

REFERENCES

(1) May, J. W. *Surf. Sci.* **1969**, *17* (1), 267–270.
(2) Dreyer, D. R.; Ruoff, R. S.; Bielawski, C. W. *Angew. Chem., Int. Ed.* **2010**, *49* (49), 9336–9344.
(3) Berger, C.; Song, Z. M.; Li, T. B.; Li, X. B.; Ogbazghi, A. Y.; Feng, R.; Dai, Z. T.; Marchenkov, A. N.; Conrad, E. H.; First, P. N.; de Heer, W. A. *J. Phys. Chem. B* **2004**, *108* (52), 19912–19916.
(4) Zhang, Y. B.; Tan, Y. W.; Stormer, H. L.; Kim, P. *Nature* **2005**, *438* (7065), 201–204.
(5) Novoselov, K. S.; Geim, A. K.; Morozov, S. V.; Jiang, D.; Katsnelson, M. I.; Grigorieva, I. V.; Dubonos, S. V.; Firsov, A. A. *Nature* **2005**, *438* (7065), 197–200.
(6) Geim, A. K.; Novoselov, K. S. *Nat. Mater.* **2007**, *6* (3), 183–191.
(7) Castro Neto, A. H.; Guinea, F.; Peres, N. M. R.; Novoselov, K. S.; Geim, A. K. *Rev. Mod. Phys.* **2009**, *81* (1), 109–162.
(8) Zhu, Y. W.; Murali, S.; Cai, W. W.; Li, X. S.; Suk, J. W.; Potts, J. R.; Ruoff, R. S. *Adv. Mater.* **2010**, *22* (46), 5226–5226.
(9) Das Sarma, S.; Adam, S.; Hwang, E. H.; Rossi, E. *Rev. Mod. Phys.* **2011**, *83* (2), 407–470.
(10) Rangel, N. L.; Seminario, J. A. *J. Phys. Chem. A* **2008**, *112* (51), 13699–13705.
(11) Wang, H.; Nezich, D.; Kong, J.; Palacios, T. *IEEE Electron Device Lett.* **2009**, *30* (5), 547–549.
(12) Dragoman, M.; Dragoman, D.; Coccetti, F.; Plana, R.; Muller, A. A. *J. Appl. Phys.* **2009**, *105* (5), 054309.
(13) Rana, F. *IEEE Trans. Nanotechnol.* **2008**, *7* (1), 91–99.
(14) Geim, A. K. *Science* **2009**, *324* (5934), 1530–1534.
(15) Yu, Q. K.; Lian, J.; Siriponglert, S.; Li, H.; Chen, Y. P.; Pei, S. S. *Appl. Phys. Lett.* **2008**, *93* (11), 113103.
(16) Kim, K. S.; Zhao, Y.; Jang, H.; Lee, S. Y.; Kim, J. M.; Kim, K. S.; Ahn, J. H.; Kim, P.; Choi, J. Y.; Hong, B. H. *Nature* **2009**, *457* (7230), 706–710.
(17) Li, X. S.; Cai, W. W.; An, J. H.; Kim, S.; Nah, J.; Yang, D. X.; Piner, R.; Velamakanni, A.; Jung, I.; Tutuc, E.; Banerjee, S. K.; Ruoff, R. S.; Colombo, L. *Science* **2009**, *324* (5932), 1312–1314.
(18) Levendorf, M. P.; Ruiz-Vargas, C. S.; Garg, S.; Park, J. *Nano Lett.* **2009**, *9* (12), 4479–4483.
(19) Yazyev, O. V.; Louie, S. G. *Phys. Rev. B* **2010**, *81* (19), 195420.
(20) Liu, Y. Y.; Yakobson, B. I. *Nano Lett.* **2010**, *10* (6), 2178–2183.
(21) Malola, S.; Hakkinen, H.; Koskinen, P. *Phys. Rev. B* **2010**, *81* (16), 165447.
(22) Grantab, R.; Shenoy, V. B.; Ruoff, R. S. *Science* **2010**, *330* (6006), 946–948.
(23) Huang, P. Y.; Ruiz-Vargas, C. S.; van der Zande, A. M.; Whitney, W. S.; Levendorf, M. P.; Kevek, J. W.; Garg, S.; Alden, J. S.; Hustedt, C. J.; Zhu, Y.; Park, J.; McEuen, P. L.; Muller, D. A. *Nature* **2011**, *469* (7330), 389–392.
(24) Kim, K.; Lee, Z.; Regan, W.; Kisielowski, C.; Crommie, M. F.; Zettl, A. *ACS Nano* **2011**, *5* (3), 2142–2146.
(25) Zeng, T. F.; Chen, G. *J. Heat Transfer* **2001**, *123* (2), 340–347.
(26) Swartz, E. T.; Pohl, R. O. *Rev. Mod. Phys.* **1989**, *61* (3), 605–668.
(27) MullerPlathe, F. *J. Chem. Phys.* **1997**, *106* (14), 6082–6085.
(28) Muller-Plathe, F.; Reith, D. *Comput. Theor. Polym. Sci.* **1999**, *9* (3−4), 203–209.
(29) Schelling, P. K.; Phillpot, S. R.; Keblinski, P. *J. Appl. Phys.* **2004**, *95* (11), 6082–6091.
(30) Lindsay, L.; Broido, D. A. *Phys. Rev. B* **2010**, *81* (20), 205441.
(31) Lindsay, L.; Broido, D. A.; Mingo, N. *Phys. Rev. B* **2010**, *82* (16), 161402.
(32) Haskins, J.; Kinaci, A.; Sevik, C.; Sevincli, H.; Cuniberti, G.; Cagin, T. *ACS Nano* **2011**, *5* (5), 3779–3787.
(33) Plimpton, S. *J. Comput. Phys.* **1995**, *117* (1), 1–19.
(34) Schelling, P. K.; Phillpot, S. R.; Keblinski, P. *Phys. Rev. B* **2002**, *65* (14), 144306.
(35) Zhang, G.; Li, B. W. *J. Chem. Phys.* **2005**, *123* (11), 114714.
(36) Ghosh, S.; Calizo, I.; Teweldebrhan, D.; Pokatilov, E. P.; Nika, D. L.; Balandin, A. A.; Bao, W.; Miao, F.; Lau, C. N. *Appl. Phys. Lett.* **2008**, *92* (15), 151911.
(37) Klemens, P. G. *Int. J. Thermophys.* **2001**, *22* (1), 265–275.
(38) Sellan, D. P.; Landry, E. S.; Turney, J. E.; McGaughey, A. J. H.; Amon, C. H. *Phys. Rev. B* **2010**, *81* (21), 214305.
(39) Nika, D. L.; Pokatilov, E. P.; Askerov, A. S.; Balandin, A. A. *Phys. Rev. B* **2009**, *79* (15), 155413.
(40) Kong, B. D.; Paul, S.; Nardelli, M. B.; Kim, K. W. *Phys. Rev. B* **2009**, *80* (3), 033406.
(41) Jauregui, L. A.; Yu, Y.; Sidorov, A. N.; Hu, J.; Yu, Q.; Lopez, G.; Jalilian, R.; Benjamin, D. K.; Delk, D. A.; Wu, W.; Liu, Z.; Wang, X.; Jiang, Z.; Ruan, X.; Bao, J. M.; Pei, S. S.; Chen, Y. P. *ECS Trans.* **2010**, *28* (5), 73–83.
(42) Cai, W. W.; Moore, A. L.; Zhu, Y. W.; Li, X. S.; Chen, S. S.; Shi, L.; Ruoff, R. S. *Nano Lett.* **2010**, *10* (5), 1645–1651.
(43) Ong, Z. Y.; Pop, E. *Phys. Rev. B* **2011**, *84* (7), 075471.
(44) Angadi, M. A.; Watanabe, T.; Bodapati, A.; Xiao, X. C.; Auciello, O.; Carlisle, J. A.; Eastman, J. A.; Keblinski, P.; Schelling, P. K.; Phillpot, S. R. *J. Appl. Phys.* **2006**, *99* (11), 114301.
(45) Maiti, A.; Mahan, G. D.; Pantelides, S. T. *Solid State Commun.* **1997**, *102* (7), 517–521.
(46) Samvedi, V.; Tomar, V. *Nanotechnology* **2009**, *20* (36), 365701.
(47) Nika, D. L.; Ghosh, S.; Pokatilov, E. P.; Balandin, A. A. *Appl. Phys. Lett.* **2009**, *94* (20), 203103.
(48) Balandin, A. A.; Ghosh, S.; Bao, W. Z.; Calizo, I.; Teweldebrhan, D.; Miao, F.; Lau, C. N. *Nano Lett.* **2008**, *8* (3), 902–907.